

**Advanced design program progress report for the
period January 1, 2004 to December 31, 2006**

ARIES-CS Compact Stellarator Study

F. Najmabadi and the ARIES Team

July 7, 2006



**Advanced Design Program
Progress Report for the Period
January 1, 2004 to December 31, 2006**

ARIES-CS Compact Stellarator Study

During this research period, we initiated and completed the ARIES Compact Stellarator study as is described below. As of the date of this progress report (6/15/06), the ARIES-CS study on schedule and is expected to be completed on time.

1. Introduction

In a stellarator, most of the confining field is produced by external coils (the poloidal field is generated by the external coils as well as the bootstrap current). Stellarators have many attractive features as a power plant because there is no large driven external current – they are inherently steady state (low recirculating power), are stable against external kink and axisymmetric modes, and are resilient to plasma disruptions.

Earlier stellarator power plant studies led to devices with large sizes compared to tokamaks. The HSR (Helias) study is based on the Wendelstein 7-X (W 7-X) plasma configuration (linked mirrors). It has an average major radius $\langle R \rangle = 22$ m for a five-field-period configuration and $\langle R \rangle = 18$ m for a recent four-field-period configuration. The Force-Free Helical Reactor (FFHR) is a 10-field period Heliotron/Torsatron ($l = 2$ stellarator) and has $\langle R \rangle = 10$ -20 m. The ARIES Stellarator Power Plant Study (SPPS), completed in 1996, was based on a four-field-period MHH (Modular Helias-like Heliac) configuration and led to an $\langle R \rangle = 14$ m device that was the first step toward a smaller-size stellarator power plant. Figure 1 compares the geometrical parameters of these devices with recent tokamak power plant studies.

The large size of these stellarators is generally dictated by the constraints imposed by the minimum distance between the plasma and the coils. In a burning plasma device and/or a power plant, the space between the plasma (i.e., last closed magnetic surface, LCMS) and the coils is occupied by the scrape-off layer, first wall, breeding blanket, shield that protects the superconducting coils, coolant manifolds, vacuum vessel, assembly gaps, coil case, and half the radial depth of the coil winding pack – typically these components require a distance of 1.5-2 m between the plasma and the middle of coil winding pack. Because the external coils generate a multipolar field and the high order harmonics of the magnetic field

decay rapidly with distance from the coils, the coil currents and irregular shape increase drastically as the distance between coils and plasma is increased. In fact, it is usually not possible to place coils at an arbitrary distance from the plasma. As such, for a given stellarator plasma/coil configuration (and aspect ratio), the average minor radius of the plasma (and the plasma-coil distance) should be increased until sufficient space is available for the above components, *i.e.*, the radial build of the device dictates a minimum average plasma minor radius. As the earlier stellarator power plant studies all had a relatively large plasma aspect ratio (see Fig. 1), the radial built constraint had led to large devices.

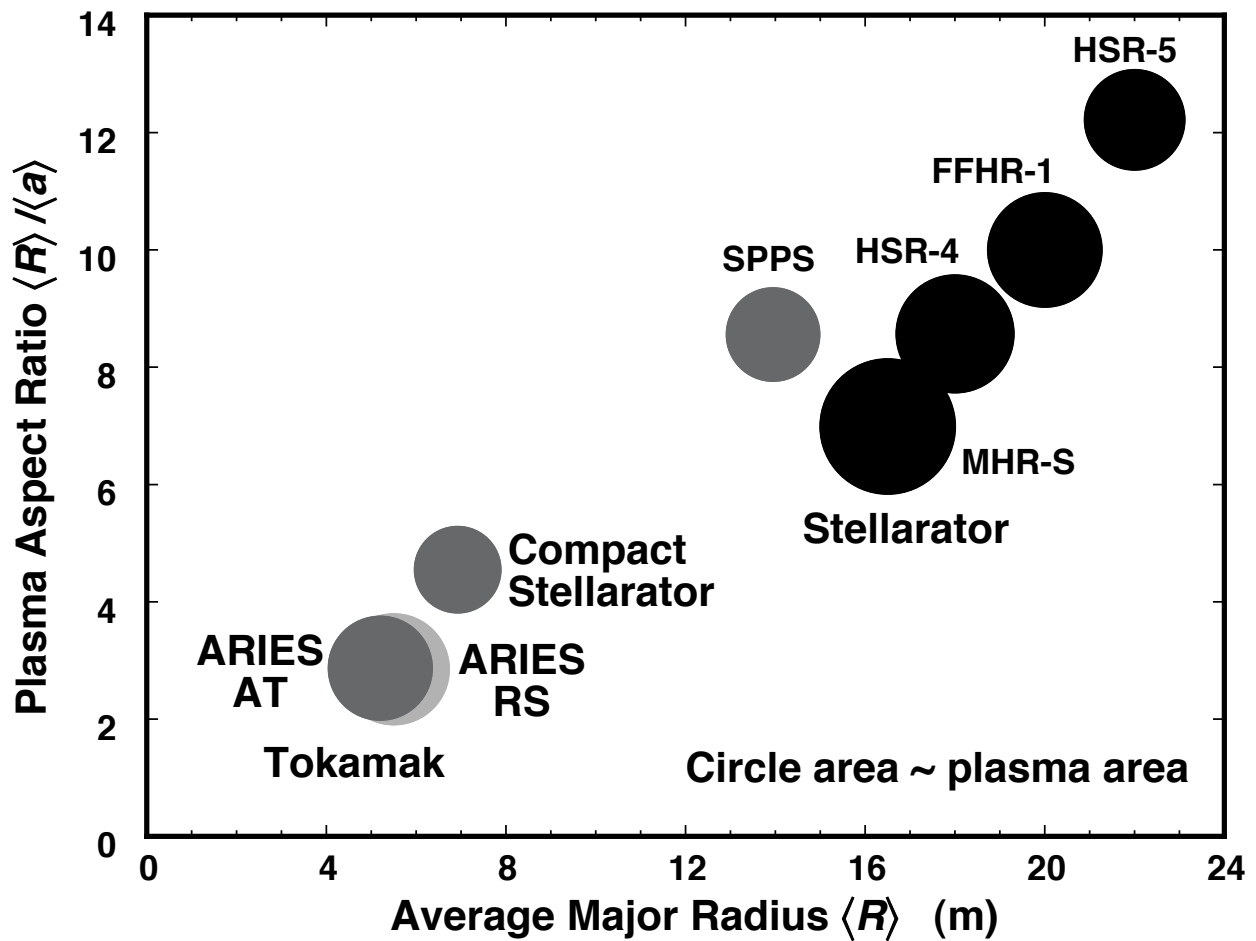


Fig. 1. A comparison of size of earlier stellarator power plant studies with more recent advanced tokamak studies, ARIES-AT and ARIES-RS. HSR-5 and HSR-4 are, respectively, 5- and 4-field period Helias configurations. The FFHR is a 10-field period Heliotron/Torsatron ($l=2$ stellarator) and SPPS is a four-field-period MHH (Modular Helias-like Heliac) configuration.

Stellarators with an underlying quasi-axisymmetric magnetic field structure have attracted intense interest in recent years because of the favorable particle drift trajectories in such configurations. In particular, compact, quasi-axisymmetric devices, which combine the feature of good particle orbits of a tokamak and the potential of being able to operate with MHD stable plasmas that are resistant to disruption at high pressure afforded by the three-dimensional shaping, open a new window of opportunity for confining steady-state, high β plasmas in magnetic fusion devices. The ability to operate at a relatively low plasma aspect ratio (~ 4 -5) is of particular importance for burning plasma devices and power plants, as they would be similar in size to tokamaks (see Fig. 1).

The stellarator configuration space is quite complex because of the large number of independent parameters (*e.g.*, β , α -particle loss, aspect ratio, number of periods, rotational transform, shear, *etc.*). Furthermore, engineering requirements and constraints such as coil topologies and maintenance/assembly approaches (which will have a major impact on in-vessel components, blanket, and power systems) may depend on details of a specific configuration. As such, optimization of any stellarator configuration represents a large number of tradeoffs among physics parameters and engineering constraints. For example, fixed-boundary analysis of a stellarator configuration may lead to a high-performance plasma configuration that cannot be produced with any practical coils and/or cannot accommodate a power-producing blanket. As such, the first phase of the ARIES compact stellarator (ARIES-CS) study was devoted to initial exploration of physics and engineering options, requirements, and constraints. In the second phase, we explored the configuration space for stellarators, aiming at configurations that satisfy physics and engineering constraints. A cost-optimization system code has also been developed and is being utilized to assess the trade-off among physics and engineering constraints in a self-consistent manner in the third and final phase of the ARIES-CS study.

We have identified several promising quasi-axisymmetric stellarator configurations (Sec. 2). Starting with an NCSX-like configuration, new configurations have been developed, others refined and improved, all aimed at low plasma aspect ratios and, hence, compact size. In each case, trade-offs among plasma parameters (*e.g.*, α -particle loss versus β) were explored. Modular coils were designed to examine the geometric complexity and the constraints of the maximum allowable field, desirable coil-plasma spacing and coil-coil spacing, and other coil parameters. Our examination of engineering options is reported in Sec. 3. In particular, we find that by employing “shield-only” zones in strategic areas, the minimum plasma-coil distance can be reduced by $\sim 30\%$. This approach, together with the relatively low aspect ratio of quasi-axisymmetric stellarators, leads to devices with an overall size similar to those envisioned for advanced tokamak power plants. An overall summary of our research to date is given in Sec. 4.

2. PLASMA CONFIGURATIONS

Stellarator configurations with an underlying quasi-symmetric magnetic field structure have attracted intense interest in recent years because of their favorable particle drift trajectories. In particular, quasi-axisymmetric (QA) configurations lead to particle orbits similar to those in a tokamak. As such, this class of configurations has the potential to combine the desirable features of tokamaks (good confinement and moderate aspect ratio) with those of large-aspect ratio stellarators (steady-state operation, stability against external kinks and axisymmetric modes, and resilience to disruptions). A relatively low aspect ratio ($A = \langle R \rangle / \langle a \rangle = 4.5$) proof-of-principle device, NCSX, based on this configuration is under construction.

Development of these and other recent stellarator configurations has been made possible by the efficient stellarator configuration optimization techniques pioneered by Nührenberg. Such an optimization involves a large number of state variables as well as constraint functions. Typical criteria used in optimizing the configuration include basic plasma properties such as the magnetic shear, magnetic well depth, and the amount of external rotational transform as well as measures of MHD stability such as external kinks, vertical displacement, and infinite- n ballooning modes, and figure of merits for transport such as the effective ripple or diffusion coefficient evaluations. For our study, confinement of α particles is the most important criterion added to the previous suite of criteria. Each criterion includes a threshold value and a weight in the optimization process – emphasizing or de-emphasizing certain properties leads to different configurations.

In arriving at a configuration, a number of optimization steps may be involved. Typically, the optimization of plasma properties, such as the amount of rotational transform or MHD stability, is accomplished first by varying the shape of the last closed magnetic surface (LCMS), which is described frequently by a double Fourier series in some toroidal and poloidal angles. Second, the coil configuration that would reproduce the desirable plasma is found by matching the normal component of the magnetic field intensity from the plasma and coils on the LCMS. Due to the discrete nature of the coils, the resulting “free-boundary” plasma equilibrium has degraded performance compared to the optimized target equilibria and some iterations are necessary to recover the optimized configuration at the end of the process. Because of our desire to explore the compact stellarator configuration space as fully as possible, our analysis to date is limited to the first two steps in the process. Because of the large computational and analysis time required for the final step of these analyses, the last step, optimization of the “free-boundary” plasma equilibria, has been performed only for the low aspect ratio MHH2 configuration.

In the optimization process, the $n = 1$ kink stability calculation was carried out by TERPSICHORE with the highest poloidal perturbation mode $m = 15$ and toroidal perturbation mode $n = 9, 8,$ and 11 for 2, 3 and 4-period devices, respectively, for a total of 91 modes in all cases. The infinite- n ballooning

calculation was carried out using COBRA along two field lines centered at $\phi = 0$ and $\pi/2$, where ϕ is the VMEC toroidal angle. VMEC equilibria were mapped to Boozer coordinates, retaining 15 poloidal modes and 9 toroidal modes in the ORBIT-3D calculation for the α -particle losses. In the evaluation of the initial collisionless losses, we used 1,024 sample particles with a uniform pitch distribution at $s = 0.25$ where s is the normalized toroidal flux. In each case, we required that both stability criteria be satisfied while α -particle losses be minimized to the extent possible. Once a configuration was found, we further carried out a complete α -particle slowing down calculation (for about two α -particle slowing down time) with a peaked, $(1-s)^8$ birth distribution and a parabolic background ion distribution. For α -particle loss calculations, the field on axis was set at 6.5 T and the major radius was adjusted such that the total volume was $1,000 \text{ m}^3$ in all the cases. The sample size for these calculations was 4,096.

An important factor in our optimization process is the recent experimental results from the Wendelstein 7-AS (W 7-AS) and Large Helical Device (LHD) stellarators. Average β values of 3.2% and 4.2% have been achieved on W 7-AS and LHD, respectively, limited only by the available heating power and perhaps the integrity of the equilibrium flux surfaces. These β values were maintained for 80-100 energy confinement times and while MHD activity apparently existed and was active in some cases, the plasmas nevertheless were quiescent and remained quasi-stationary. In both cases, the achieved experimental values were higher than those predicted from linear stability theory (e.g., 3.2% achieved β in W 7-AS versus 2% for the theoretical prediction). These results led us to explore new configurations with more emphasis on the quality of flux surfaces and transport, particularly the confinement of α particles, than strict adherence to linear MHD stability requirements. As will be discussed later, confinement of fast α particles is of great importance in a burning plasma and/or fusion power plant.

Three distinct classes of QA configuration have been considered for the ARIES-CS. First is the NCSX-class configuration that maintains the basic characteristics of the NCSX plasma and coils: it provides a good “balance” between quasi-axisymmetry and MHD-stability considerations, it has been shown to have high β limits against linear MHD modes, and particular coils have been designed that recover all of the desirable plasma properties. For the NCSX-class, we have developed new configurations with $A = 4.5$ with coils sufficiently removed from the plasma. Three variants of this configuration have been developed to explore the trade-off between confinement of fast α particles and linear MHD stability (Sec. 2.1).

The second class of configurations is MHH2, which aims at developing a very low aspect ratio geometry with relatively simpler coils (discussed in Sec. 2.2) to explore how compact a compact stellarator power plant can be. The third class, SNS, is aimed at developing a configuration with excellent

flux surface quality and nearly flat rotational transform (Sec. 2.3) to explore how good and robust flux surfaces can be designed. In both cases, strict adherence to linear MHD stability is deemphasized.

2.1. NCSX-CLASS CONFIGURATIONS

The first variant of NCSX-class configurations is the scale-up of NCSX to a power plant with a plasma aspect ratio of 4.5. The boundary shape is designed such that the plasma is stable, based on numerical calculations, to vertical displacements without the need of feedback stabilization, and is also stable to the $n = 1$ external kink mode and ballooning modes at $\langle\beta\rangle = 4\%$. The configuration has excellent quasi-axisymmetry, measured by the effective ripple, $\epsilon_{\text{eff}} < 1\%$ everywhere. The shaping of the plasma results in a vacuum rotational transform from 0.42 to 0.48, which accounts for more than 70% of the total. The drawback of this configuration is its large α -particle loss of $\sim 18\%$. Several coil designs were produced with different Δ_{min} , the distance between the LCMS and the middle of the winding pack (parameterized by coil aspect ratio, $A_c = \langle R \rangle / \Delta_{\text{min}}$). The geometry of the LCMS as well as a typical coil configuration is shown in Fig. 2. An important parameter is the ratio of the maximum field on the coil, B_{max} , to the field at the plasma axis, B_0 (B_{max} directly impacts the choice, design, and cost of superconducting magnets). Table 1 show the trade-off between increasing Δ_{min} and the resultant increase in B_{max}/B_0 – there is an optimum coil aspect ratio, ~ 5.9 here, above which B_{max}/B_0 increases rapidly. This is an optimum point as it allows for the largest Δ_{min} with the smallest penalty in coil manufacturing and cost as related to B_{max} .

Two new variants of NCSX-class configuration were developed in order to reduce α -particle losses. The importance of the α -particle loss resulting from the breaking of axisymmetry has been realized for quite some time. Efforts to use various techniques to minimize their losses in the configuration design have been attempted. We have found that introducing a bias in the magnetic spectrum in favor of the $B(0,1)$ component reduces the α -particle loss substantially. (Note, $B = \sum B(m,n) \cos [m\theta - (n - \iota m)\varphi]$). The first of these two variants, called N3ARE, has a rotational transform (Fig. 3) similar to that of NCSX. Eight major non-axisymmetric components in the magnetic spectrum are plotted as function of the normalized toroidal flux in Fig. 4, showing enhanced values of $B(0,1)$ and $B(1,1)$ and reduced values of $B(2,1)$ and $B(3,2)$ components. In this configuration, the external kinks and infinite- n ballooning modes are marginally stable at $4\% \beta$ with no conducting wall. The α -particle loss is reduced to $3\% - 4\%$ in this configuration.

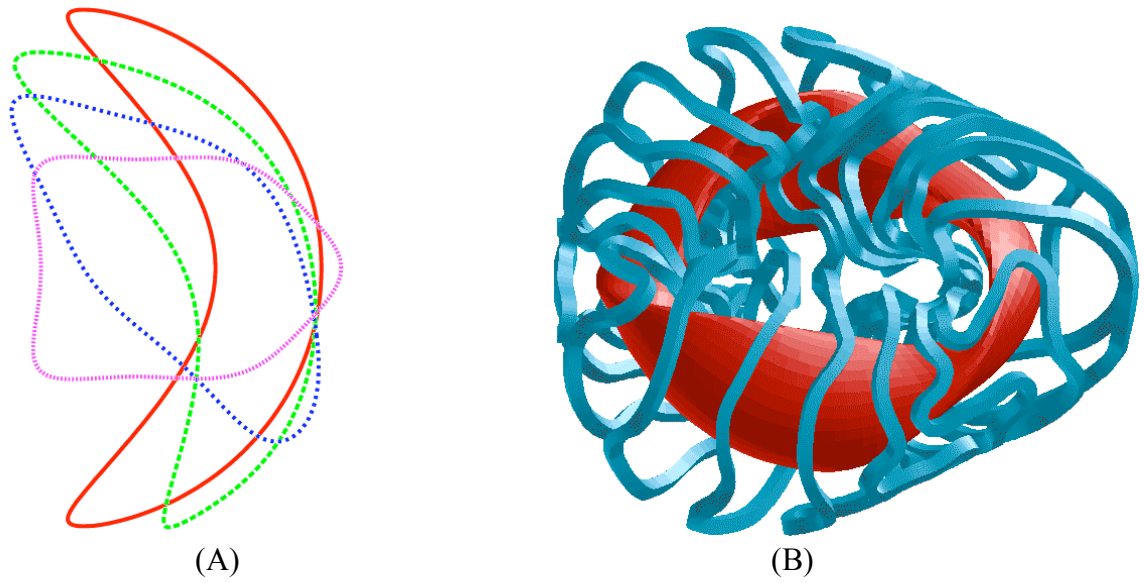


Fig. 2. A) Cross section of the LCMS at four toroidal sections for the NCSX-scale-up configuration. B) A typical coil design for this configuration that allows sufficient space between the coils and the plasma.

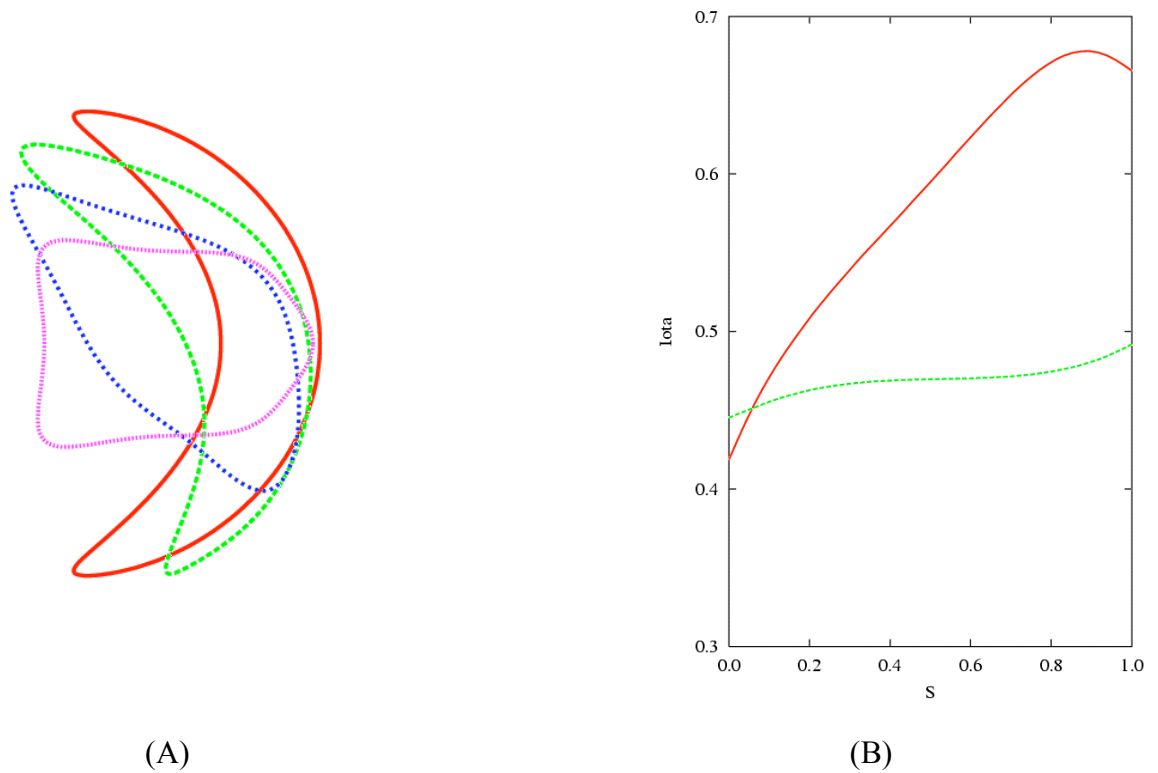


Fig. 3. A) Cross section of the LCMS at four toroidal sections and B) the rotational transform as a function of normalized toroidal flux s for the N3ARE configuration. The dashed line is the rotational transform from external coils (or transform at $\beta = 0$) and the solid line is the total rotational transform (ι) including the bootstrap current contribution at $\beta = 4\%$.

Table 1. Impact of increased plasma-coil distance, Δ_{\min} , parameterized by coil aspect ratio on B_{\max}/B_0 for an NCSX scale-up configuration.

Coil Aspect Ratio, $A_c = \langle R \rangle / \Delta_{\min}$	6.82	6.10	5.89	5.67
B_{\max}/B_0 (for a 0.3 m x 0.3 m winding)	2.49	2.57	2.63	2.85

As experimental results show that stellarator β limits may be better correlated to the quality of equilibrium flux surfaces as opposed to linear MHD stability limits, the second new variant, KQ26Q, aims at good equilibrium flux surface quality. The external transform is increased to remove the $m = 6$ rational surface and to move the $m = 5$ surface to the core relative to the N3ARE and NCSX scale-up configurations (see Figs. 5 and 6). This configuration may be unstable to free-boundary modes for $\beta = 4\%$. All three variants of NCSX-class configurations have coils that have similar overall coil parameters like minimum bend radius, total coil currents, coil aspect ratio and B_{\max}/B_0 .

2.2. MHH2 CONFIGURATION

The plasma aspect ratio (and number of field periods) has a dramatic impact on the size of the device. While NCSX-class configurations can be developed with smaller aspect ratio and/or smaller number of field periods, the necessary coils were becoming exceedingly difficult to design and good “quasi-axisymmetry” was difficult to obtain. We have identified a new class of 2-field-period configurations, generally known as MHH2, that have aspect ratios down to only 2.5, yet they possess excellent quasi-axisymmetry and very low field ripples. Fig. 7 shows the LCMS of a typical example that is designed to have a nearly flat, but slightly negative, rotational transform profile ranging from 0.4 on the magnetic axis to 0.35 at the boundary for $\beta = 0$. The configuration is also optimized such that it has good quasi-axisymmetry at 5% β with a rising rotational transform (including the bootstrap current contribution). In the fixed-boundary calculations, a linear iota profile increasing from 0.32 on the axis to 0.58 at the boundary was assumed at full β without considering any specific pressure profile and collisionality (*i.e.*, the bootstrap current). The largest non-axisymmetric component ($\sim 1.7\%$) in the magnetic spectrum is the principal mirror term, *i.e.*, $m = 0$, $n = 1$. As observed in many of our configurations, the mirror term plays an important but not yet fully understood role in helping reduce α -particle losses.

This configuration was reproduced in a 16-coil design with the total rotational transform profile (sum of external and bootstrap) being very close to a linear profile (See Fig. 7). The resulting configuration has excellent QA, low effective ripple ($< 0.8\%$) and α -particle losses $< 5\%$. There are four distinct types of

coils in each of the half periods with the coil aspect ratio of 5.5. The ratio of the plasma major radius to the minimum radius of curvature of these coils is about 13, indicative of the relatively simpler coils with “smaller” twist, as can be seen in Figs.7 and 8.

2.3. SNS-QA CONFIGURATION

The integrity of equilibrium flux surfaces places a limit on the attainable β because the Shafranov shift of the magnetic axis may cause flux surfaces to collapse if the pressure become excessive or the formation of magnetic islands may short circuit plasma confinement by allowing heat to flow along a separatrix if low order resonances exist. If resonances are too close together, the fields may also become stochastic.

The existence of rational surfaces cannot be avoided in a stellarator. Most conventional stellarators are designed for the condition of zero net current, in which case the rotational transform at finite beta deviates from that in a vacuum only by the effect of the Pfirsch-Schluter current, which is generally small. The vacuum transform in these devices was normally chosen carefully to avoid low order resonances to guarantee good flux surfaces. In a QA stellarator, bootstrap currents of the magnitudes close to those in tokamaks are expected. Their presence modifies the overall rotational transform and the resulting shear, which could be large and would draw many of the resonances close to each other. The impact of resonances on the flux surface integrity may be minimized by a carefully tailored rotational transform profile.

One way to avoid low order rational surfaces in a QA stellarator is to make the profile of the rotational transform due to plasma shaping a strongly decreasing function of radius so that when the internal transform is superimposed at a finite plasma pressure, the total transform will have a small but positive slope. When chosen properly, the total transform could be in a region free of low order resonances. The shear may be made small enough to maintain adequate spacing among the remaining resonances to assure an ordered field line topology. The positive shear would ensure stability against tearing modes. One example of such configurations with aspect ratio 6 and three field periods is given in Fig. 9. At 6% β the total transform is expected to be 0.53 on the magnetic axis and 0.55 at the boundary (see Fig. 9) with an overall shear of only about 5%. There are essentially no low order resonances, and the second and third order resonances are near the magnetic axis and are not important for the quality of the flux surfaces. Calculation using the PIES¹⁸ code, which does not assume the existence of nested flux surfaces, has demonstrated the integrity and excellence of the flux surface at 6% β . This configuration has good QA quality, low effective ripple ($< 0.4\%$), and α -particle losses $\leq 10\%$.

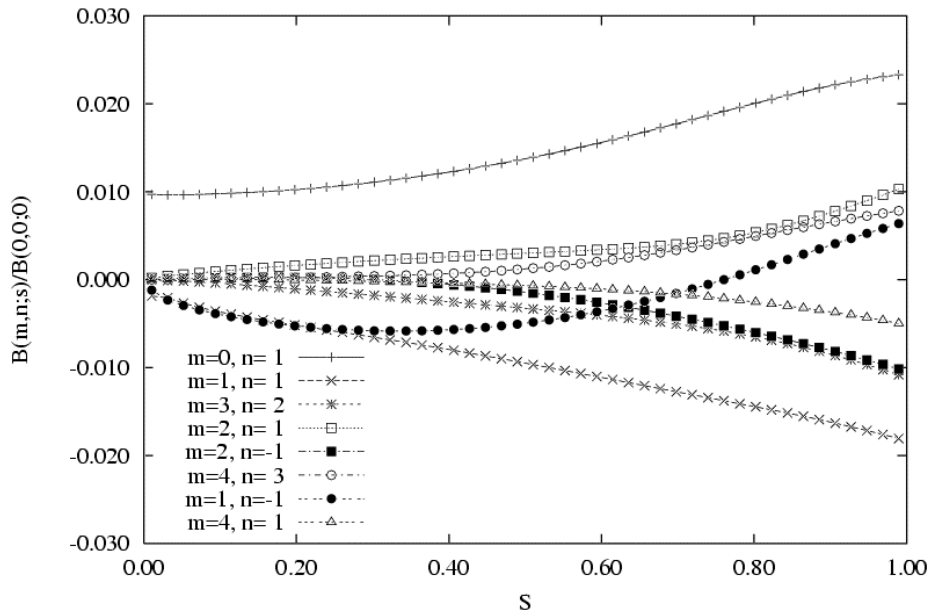


Fig. 4. Harmonic contents in the Boozer magnetic spectrum for the N3ARE configuration as a function of the normalized toroidal flux, s . Note the enhanced $B(0,1)$ and $B(1,1)$, and reduced $B(2,1)$ and $B(3,2)$ components.

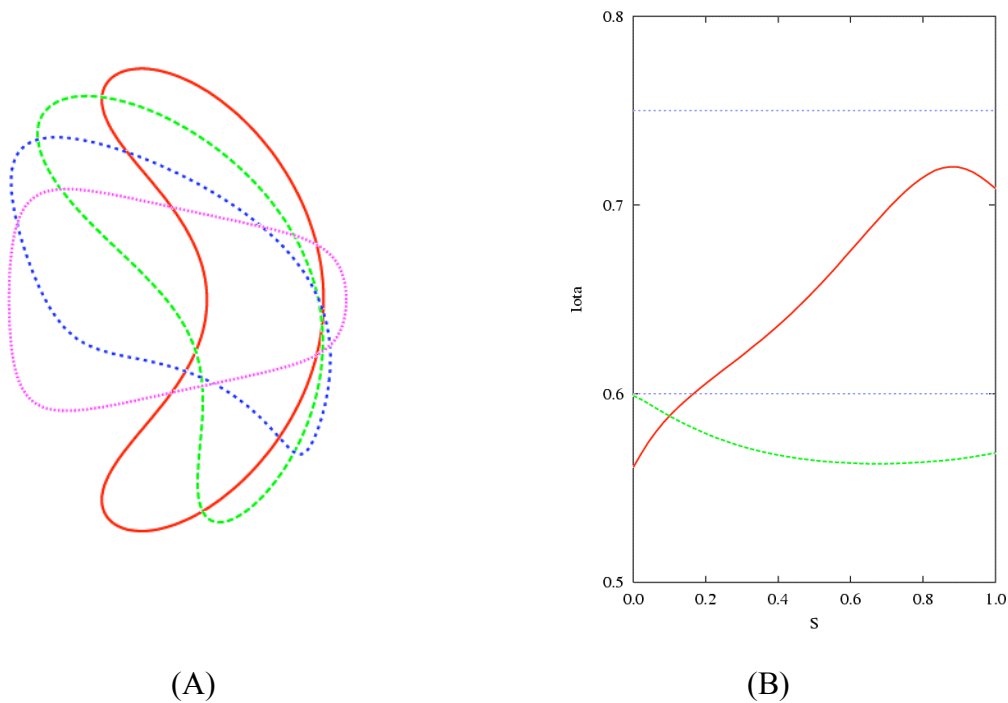


Fig. 5. A) Cross section of the LCMS at four toroidal sections and B) the rotational transform as a function of normalized toroidal flux s for the KQ26Q configuration. The dashed line is the rotational transform from external coils (or transform at $\beta = 0$) and the solid line is the total iota including the bootstrap current contribution at $\beta = 4\%$.

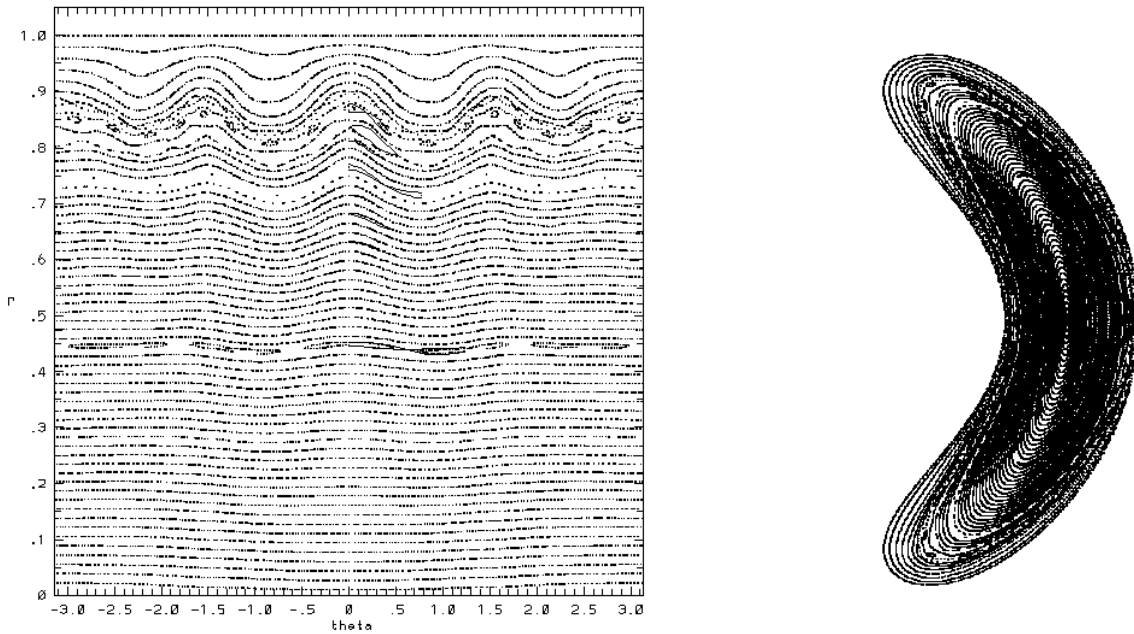


Fig. 6. Equilibrium flux surfaces of the KQ26Q configuration as calculated by PIES at $\beta = 4\%$ showing excellent equilibrium flux surface quality.

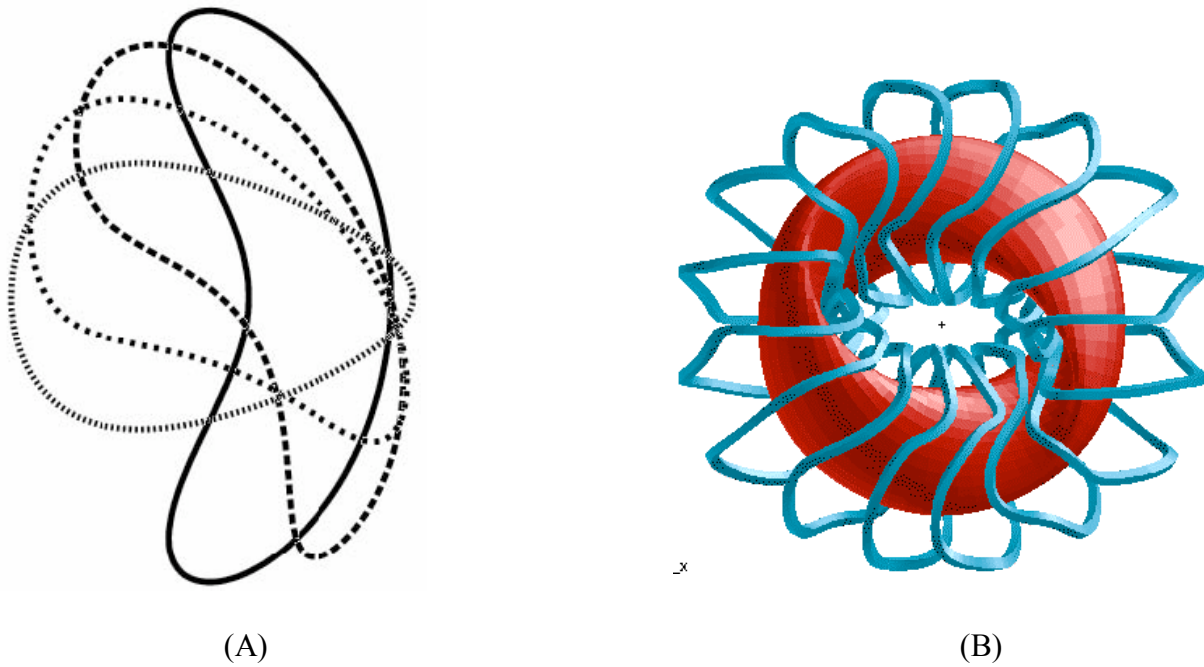


Fig. 7. A) Cross sections of the LCMS at four toroidal sections and B) discrete coil designs for the MHH2 configuration (2 field period, plasma aspect ratio of 2.5 [2.7?]).

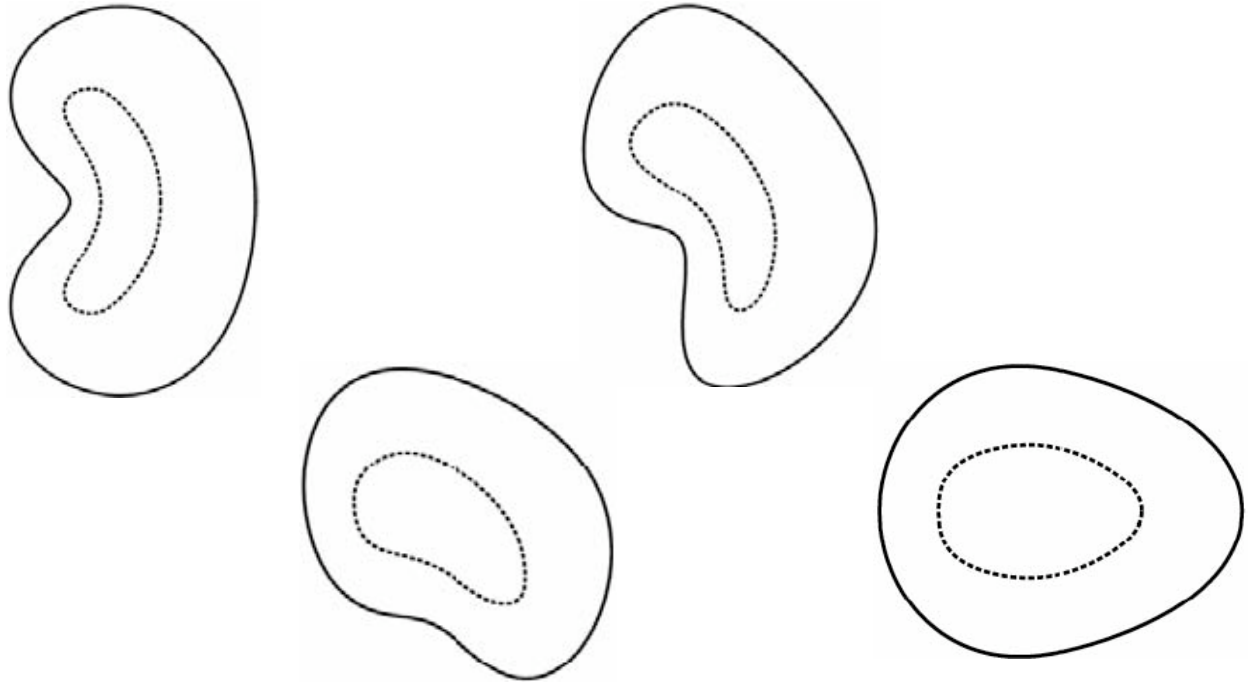


Fig. 8. Coil winding surface and the last closed magnetic surface of the MHH2 configuration at four equally spaced toroidal planes over a half-period. The LMCS is found by VMEC at 5% β .

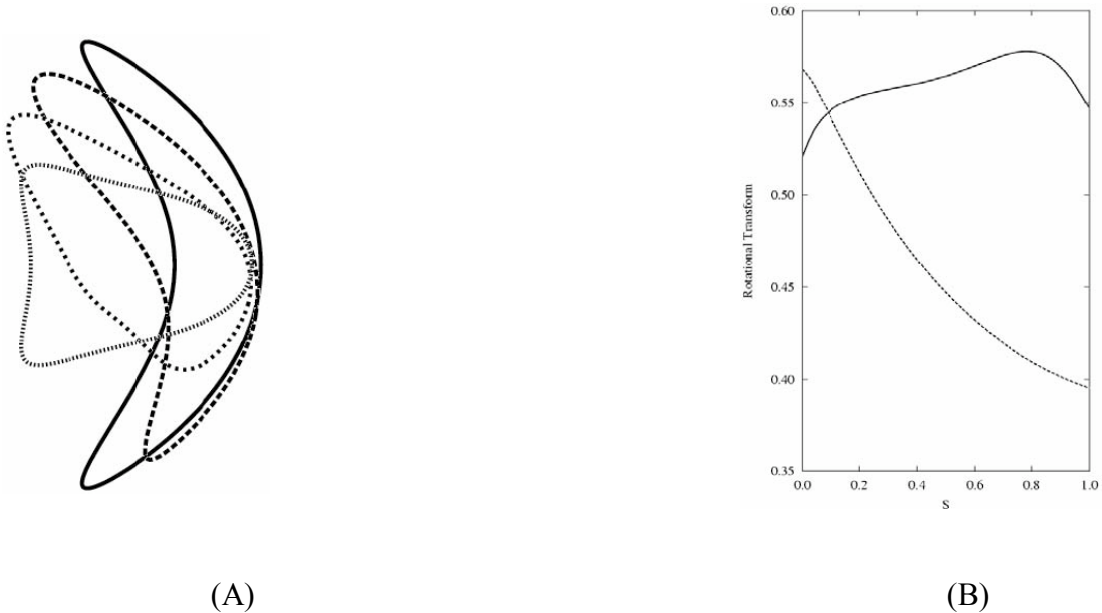


Fig. 9. A) Cross section of the LCMS at four toroidal sections and B) the rotational transform as a function of the normalized toroidal flux s for a 3-field-period SNS-QA configuration. The dashed line is the rotational transform from external coils (or transform at $\beta = 0$) and the solid line is the total iota including the bootstrap current contribution at $\beta = 6\%$. Note that there are essentially no low order resonances.

3. ENGINEERING OPTIONS

The choice of breeding blanket and shield plays an important role in optimizing the stellarator configuration for a power plant. First, the needed space between the plasma and the coil (scrape-off-layer, first wall, blanket, shield, *etc.*) is a critical parameter in determining the external coil design and overall device optimization – the device major radius directly scales with this minimum stand-off, Δ_{\min} . This distance is set by the nuclear performance of the blanket/shield region, *i.e.*, tritium breeding and magnet protection. The blanket should also be optimized in order to maximize its thermal performance (*i.e.*, heat load capability and thermal efficiency) as it has a direct impact on the fusion power and machine size. Second, the constraints on the external coils (*e.g.*, bend radius, inter-coil spacing, support structure) play an important role in setting the magnetic field strength and device optimization. The divertor heat removal capability and its location impose another set of important constraints. Lastly, all of these constraints are directly coupled to the proposed procedures for the machine assembly and the scheduled maintenance of the power core (regular replacement of first wall and blanket).

Different maintenance schemes were considered in order to provide a broad range of possibilities to accommodate the physics optimization of the number of coils and the machine size. Port-based maintenance (Sec. 3.1) is the preferred scheme, whereby replacement of the blanket modules is done through a limited number of designated maintenance ports.

Several blanket designs were considered aiming at high thermal performance, compatibility with machine assembly and maintenance, and minimization of the radial build (*i.e.*, Δ_{\min}). A novel approach was developed in ARIES-CS in which the blanket at the critical areas of minimum stand-off is replaced by a highly efficient tungsten-carbide-based (WC) shield, thereby reducing Δ_{\min} by 30% to 50% (Sec. 3.2). The reference blanket option is a dual-coolant concept with self-cooled Pb-17Li zones and He-cooled ferritic steel structure. A self-cooled Pb-17Li blanket with SiC_f/SiC composite as structural material, based on the ARIES-AT blanket design, is maintained as a back-up, high-risk, high-payoff option. This latter blanket option allows for high operation temperature and high performance (with a power cycle efficiency ~55-60%), but carries a higher development risk mostly due to SiC_f/SiC material development. Sec. 3.4 overviews a divertor design that can accommodate the expected heat flux. One key issue that needs further attention is the accommodation of the high-energy α -particle losses, and in particular, armor survival issues (Sec. 3.5).

The superconducting magnet design for a compact stellarator is reviewed in Sec. 3.6. In particular, because of the irregular geometry and small bend radius, development of inorganic insulators is necessary in order to access maximum field of >9 T.

Most of the engineering analysis was performed for the NCSX-class configurations as they were developed earliest in our research. Unless otherwise stated, these results are equally applicable to the MHH2 configuration.

3.1. ASSEMBLY AND MAINTENANCE

Two assembly and maintenance schemes are being considered during the second phase of the study in order to provide a broad range of possibilities to accommodate the physics optimization of the number of coils and the machine size. Port-based maintenance is the preferred scheme, described in more detail below, whereby replacement of the blanket modules is done through a limited number of designated maintenance ports. As an alternative, field-period maintenance scheme, is also considered with replacement of integral units based on a field-period including disassembly of the modular coil system. The choice of assembly/maintenance scheme would dramatically affect the machine layout and the design of various components.

Port-based maintenance involves the replacement of blanket using an articulated boom through a number of designated ports. For an NCSX-like configuration with three field periods, one maintenance port per field period is assumed; for an MHH2-like two-field period configuration, more than one port per field period would be required but there is substantial space between adjacent coils and this can readily be accommodated. For this maintenance scheme, the vacuum vessel is internal to the coils and serves as an additional shield for the protection of the coils from neutron and gamma irradiation, as illustrated in Figs. 10 and 11 for the three-field period configuration. In this arrangement the modular coils are kept at cryogenic temperatures during maintenance. A key feature of the layout is the desire to separate the hot core (including the shield and manifold, which are lifetime components) from the cooler vacuum vessel to minimize thermal stresses. In the absence of disruption, the hot core does not need to be strongly attached to the vacuum vessel, being instead vertically self-supported. In this case, no disassembling and re-welding of the vacuum vessel are required for blanket maintenance. The maintenance ports are arranged between adjacent coils at locations with large port space and large plasma cross section. Transfer casks can be attached to the outside flange of the port, and a system of double doors can be employed to avoid any spread of radioactivity (dust, tritium) into the containment building. The load capacity and required reach of the boom limit the weight ($\sim 5,000$ kg) and size of the blanket modules.

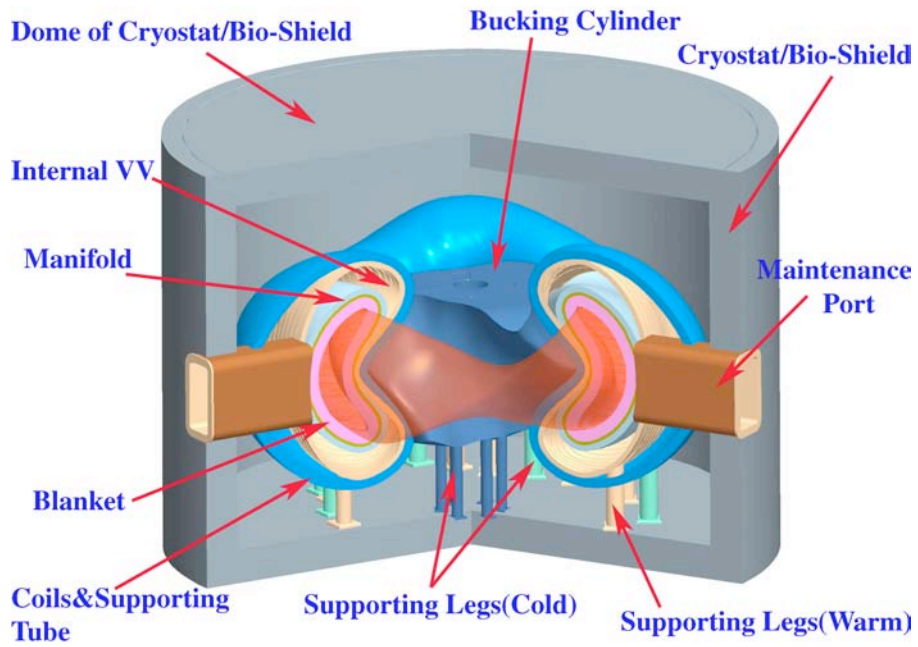


Fig. 10. Layout of power plant core showing the coil structure and the maintenance ports.

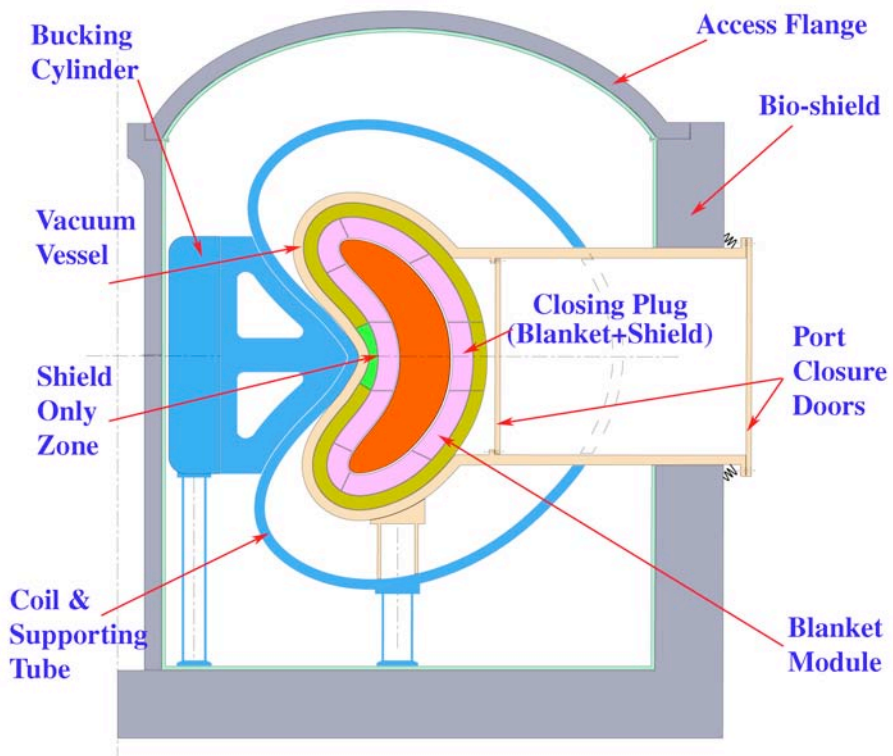


Fig. 11. Layout of 3-field period power core for port-based maintenance.

The reference blanket option is a dual-coolant concept with self-cooled Pb-17Li zones and He-cooled ferritic steel structure. Cutting and re-welding the coolant pipes for blanket module removal and replacement are done from the outside of the tubes (in-bore cutting is an alternate option). The coolant pipe routing for both the He and Pb-17Li flows is done through concentric pipes with sliding seals for the inner tube at the disassembly location. In order to have access for performing these procedures a neighboring module must be removed first. Thus, the maintenance scheme requires in-series removal of specific modules in order to access a given module. The coolant piping cut is performed at the back of the shield where the He production is small enough to allow re-welding (assumed as < 1 appm He). In the case of the He coolant piping, neutron streaming is a concern; a solution is to increase the feed pipe size and introduce an additional shield ring.

3.2. BLANKET

The reference blanket option is a dual-coolant concept with self-cooled Pb-17Li zones and He-cooled ferritic steel structure which is described in details here. A self-cooled Pb-17Li blanket with SiC_f/SiC composite as structural material, based on the ARIES-AT blanket design is maintained as a back-up option. It allows for high operation temperature and high performance (with a power cycle efficiency ~55-60%) but carries a higher development risk mostly due to SiC_f/SiC material development)

The dual coolant concept utilizes He to cool the ferritic steel (FS) structure (including the first wall) and slowly flowing Pb-17Li as self-cooled breeder in the inner channels, which can be operated at a higher temperature than the structural blanket walls to maximize the power cycle efficiency. Use of He coolant for the first wall/structure also facilitates the pre-heating of the blankets before the liquid breeder is filled in, serves as guard heating in case the liquid breeder can not be circulated, and provides independent and redundant decay-heat removal in case the liquid metal loop is not operational. In addition, cooling the first wall region of the blanket (where the heat load is highest) with helium (instead of a liquid metal) avoids the need for an electrically insulating coating in this high velocity region to prevent the large MHD pressure drop associated with liquid metal flow. Such a dual coolant concept was originally developed as part of the ARIES-ST study and then at FZK in Germany.

Internals of the blanket module is shown in Fig. 12, with both He and Pb-17Li fed to the back of the blanket module through concentric pipes. The dimensions of the module are about 2 m poloidally by 2 m toroidally. The helium coolant (assumed at 8 MPa) is routed to first cool the first wall in a single pass with an alternating toroidal flow configuration to create a more uniform temperature (and reduce thermal stresses); it is then routed in a combination of series and parallel flow to cool all other structural walls (see Fig. 12). The Pb-17Li flows slowly (~10 cm/s or less) in the large inner channels in a two-pass poloidal configuration, as illustrated in Fig. 12. The Pb-17Li channels are lined with a SiC insulating

layer (with no structural function as the thin Pb-17Li layer and the bulk Pb-17Li are pressure-balanced through a thin slot in the SiC), as illustrated in Fig. 13. This layer provides the key thermal insulation function to allow high temperature ($\sim 700^{\circ}\text{C}$) Pb-17Li in the channel while maintaining the Pb-17Li/steel interface temperature below its compatibility limit which appears to be more limiting than steel's maximum operating temperature.

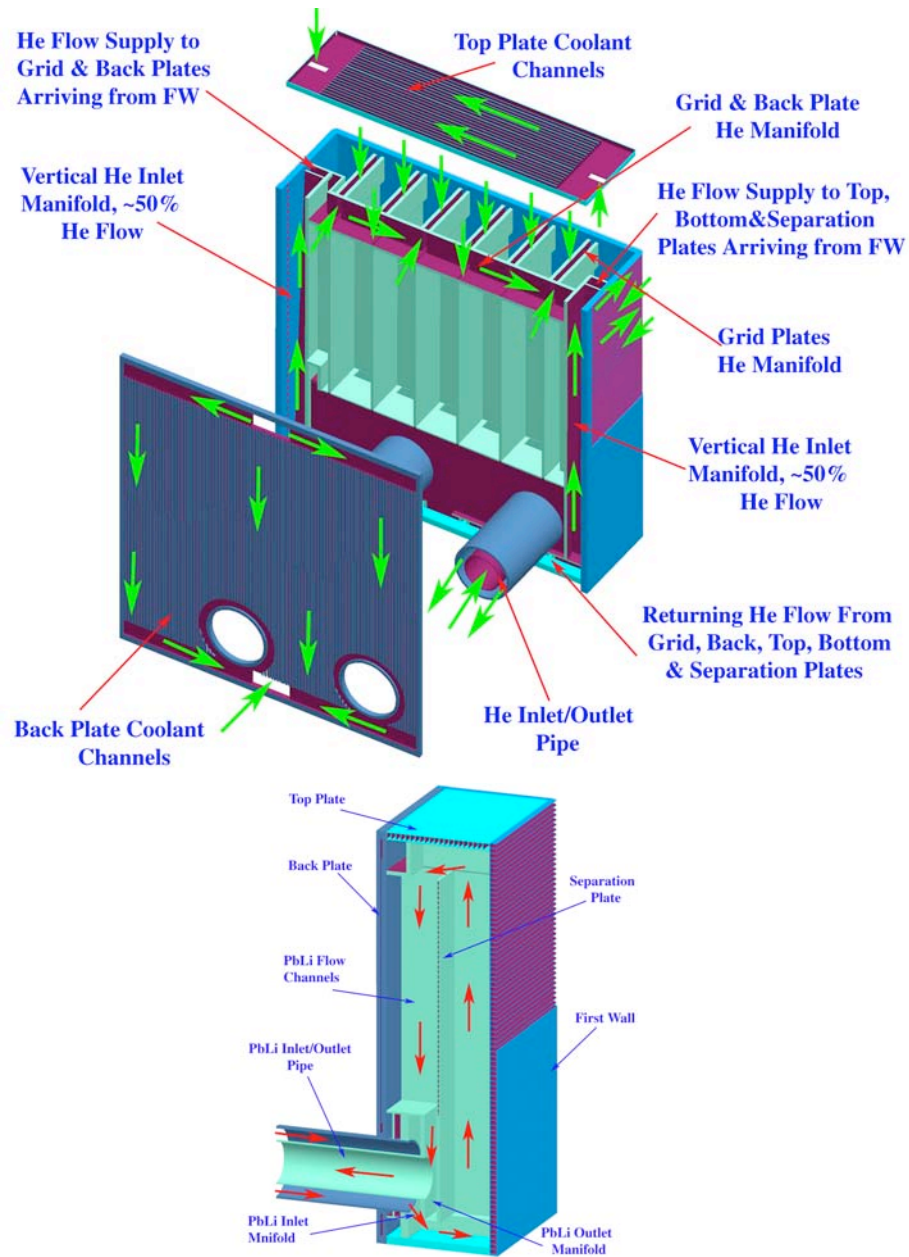


Fig. 12. Schematic of He coolant flow in dual-coolant blanket module.

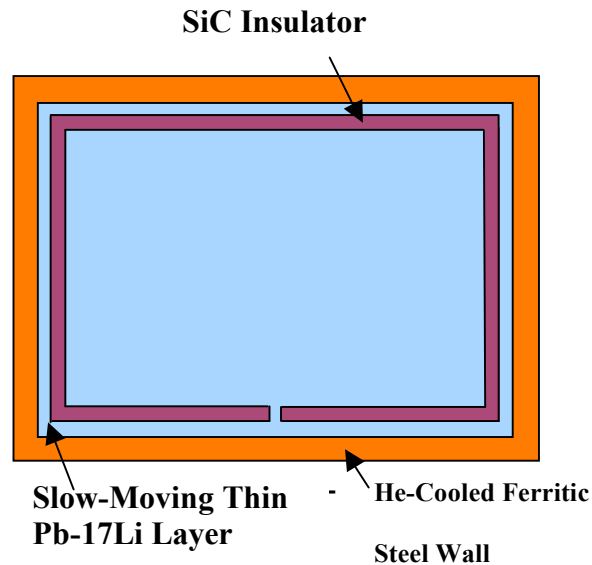


Fig. 13. Schematic of SiC layer in inner Pb-17Li channel.

A key engineering parameter for a compact stellarator is the minimum coil-plasma distance, Δ_{\min} . A novel approach has been developed where the blanket at the critical area surrounding Δ_{\min} has been replaced by a highly efficient WC shield. These modules utilize WC in a He-cooled ferritic steel box, optimized to provide shielding comparable to the breeding blanket but with a much reduced module radial thickness (by as much as 50 cm). These shield-only regions, as illustrated in Fig. 11, would cover about 5% of the first wall area. The full blanket region covers about 85% of first wall area and provides most of T breeding (local TBR = 1.25). A transition region with a local TBR=0.85 exists between adjacent full blanket and shield-only regions leading to an overall TBR of ~ 1.1 and an overall energy multiplication of 1.15. Within the blanket region, there are two breeding zones, each 25 cm. The inner zone provides approximately 70% of the tritium breeding capability.

We developed a unique approach that helps model complicated geometries, such as ARIES-CS, for the 3-D MCNPX Monte Carlo code. This approach allows fully accurate 3-D model directly from the CAD system to MCNPX in much less time than was previously possible. 3-D neutronics analysis of the exact geometry of ARIES-CS components were performed for a full coverage blanket. A fairly good agreement with the 1-D results was obtained for the local TBR, nuclear heating, and FW damage.

Activity, decay heat, and waste disposal rating (WDR) for the various components and constituents were estimated. The WC-shield was segmented into replaceable and permanent components to minimize the waste stream volume. The blanket and divertor are replaceable components with an

end-of-life fluence of 15 MWa/m^2 , while the FS shield, VV, and magnet are life-of-plant components. The WC shield generates high activity and decay heat that drop slowly over time compared to the surrounding blanket and shielding components. The WDR is less than unity for all components, meaning the activated materials qualify as low-level waste at the end of a 100 y storage period after decommissioning (approximately, 34% Class A and 66% Class C waste under US regulations).

The blanket is coupled to a Brayton cycle through a heat exchanger where both coolants (He and Pb-17Li) transfer their energy to the cycle working fluid (He). For the Pb-17Li, use of the SiC insulator in the return inner channel of the concentric coolant access pipes would also allow the use of FS for the coolant piping; however, the heat exchanger tubes would have to be made of higher temperature material (most probably a refractory alloy, such as niobium or tantalum). Use of niobium or tantalum alloys, which have a high tritium permeability, is also considered for a permeator-based tritium recovery system from the hot Pb-17Li, which would then be routed to the heat exchanger with a minimal remaining tritium concentration (thus minimizing the tritium permeation there). The Brayton cycle considered for this study includes 3 compression stages and a single expansion stage with a gross thermal efficiency of 41%.

Detailed thermal-hydraulic analyses were performed for the dual-coolant blanket coupled to the Brayton cycle. The analysis aimed at maximum net thermal efficiency for different neutron wall loads (and corresponding plasma heat fluxes) for a given set of constraints, including a maximum Pb-17Li/FS interface temperature $< 500^\circ\text{C}$ and a radially averaged FS temperature at the FW $< 550^\circ\text{C}$. These were found to limit the maximum wall loading to $\sim 5 \text{ MW/m}^2$. (average wall load of $\sim 3.3 \text{ MW/m}^2$). For the divertor region, a fractional He pressure drop of ~ 0.1 was deemed reasonable. However, for the blanket, the analysis was carried out by trying to limit the fractional He pressure drop to ~ 0.05 .

It is desirable to minimize the thermal conductance of the SiC insulation region in the inner channel to allow for a high Pb-17Li outlet temperature while accommodating the 500°C Pb-17Li/FS maximum interface temperature limit. The overall thermal conductance of this insulation region was set as $200 \text{ W/m}^2\text{-K}$ under the assumption that it could be credibly achieved (*e.g.* through a 5 mm thick layer of porous SiC with a conductivity of 1 W/m-K assuming a uniform bulk Pb-17Li temperature). Although the MHD pressure drop of Pb-17Li in bare inner channels could be acceptable ($\sim 0.1\text{-}0.5 \text{ MPa}$), the uncertainty linked with turning flows could increase the total pressure to an unacceptable value. Thus, the SiC layer also plays an important electrical insulation function, which was included in the pressure drop calculations.

The optimization was done by considering the net efficiency of the Brayton cycle for a 1,000 MWe power plant. The friction power from the He flow in the blanket and divertor in the calculations is added to the fusion thermal power for these calculations and the net efficiency is estimated from the net

electrical power (gross electrical power minus pumping power). The results are summarized in Fig. 14. The net efficiency decreases from ~42% to ~38% as the maximum wall load is increased from 2 to 5 MW/m². The corresponding gross thermal efficiency is typically about 2 points higher than the net efficiency. The blanket design parameters, including the He and Pb-17Li thermal-hydraulic parameters, are summarized in Table 2 for such a case.

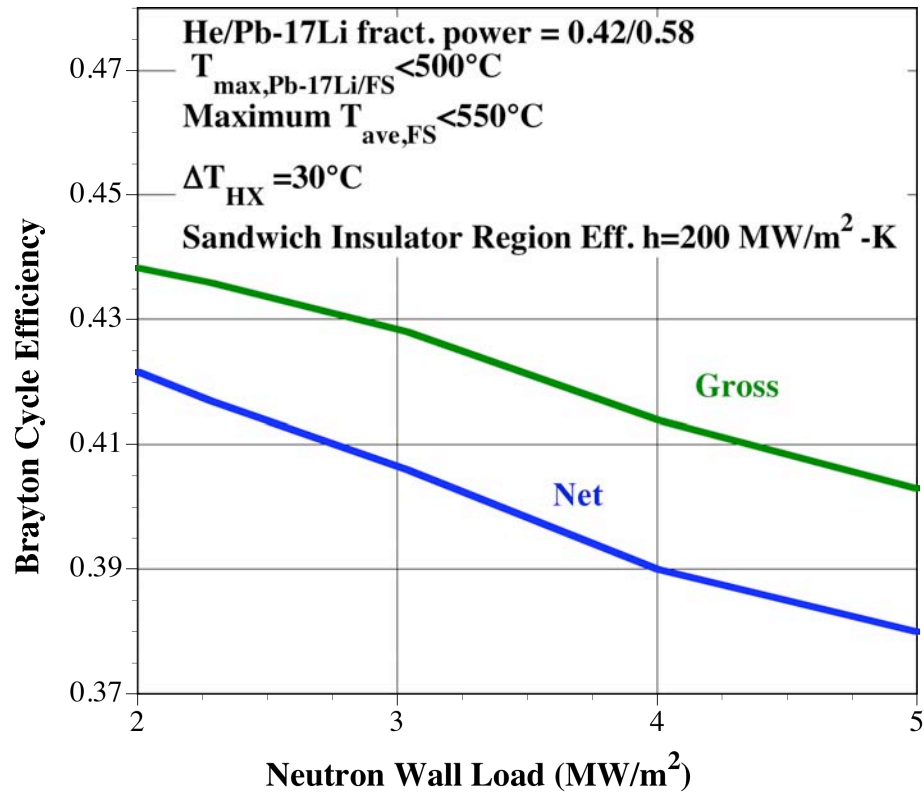


Fig. 14. Gross and net (including pumping power) Brayton cycle efficiency as a function of neutron wall load.

Table 2. Summary of Typical ARIES-CS Blanket for example 3-Field Period Configuration**Blanket**

Typical Module Dimensions	2 m x 2 m x 0.62 m
Tritium Breeding Ratio	1.1
Fusion Thermal Power in Blanket	2267 MW

Blanket Pb-17Li Coolant

Pb-17Li Inlet Temperature	502°C
Pb-17Li Outlet Temperature	710°C
Pb-17Li Inlet Pressure	1 MPa
Typical Inner Channel Dimensions	0.26 m x 0.24 m
Thickness of SiC Insulator in Inner Channel	5 mm
Effective SiC Insulator Region Conductivity	200 W/m ² -K
Average Pb-17Li Velocity in Inner Channel	~0.1 m/s
Total Thermal Power removed by Pb-17Li	1315 MW
Pb-17Li Total Mass Flow Rate	35,285 kg/s
Pb-17Li Pressure Drop	0.9 kPa
Pb-17Li Pumping Power	~ 2 kW
Maximum Pb-17Li/FS Temperature	500°C
Maximum FS Temperature in Blanket	

Blanket He Coolant

He Inlet Temperature	368°C
He Outlet Temperature	486°C
He Inlet Pressure	8 MPa
Typical FW Channel Dimensions	2 cm x 3 cm
He Velocity in First Wall Channel	71 m/s
Blanket Pressure Drop	0.37 MPa
Total Thermal Power removed by He	952 MW
Total Mass Flow Rate	1740 kg/s
Pumping Power	128 MW
Maximum Local FS Temperature at FW	608°C
Radially Averaged FS Temperature at T _{max} Location	560°C

3.4. Plasma-Facing Components

A suite of codes are utilized to carry out the divertor physics studies for the complex 3D magnetic geometry of a compact stellarator. The combination of VMEC and MFBE calculates the magnetic field on a 3D grid both inside and outside the last closed magnetic surface (LCMS), including finite plasma β effects such as the bootstrap current. The GOURDON code is used to trace magnetic field lines from the LCMS to the target plates and the first wall. The GEOM code specifies the location and geometry of the plates and the first wall. Together these codes determine the footprints of the field lines on the target. Iterations between GOURDON and GEOM are performed until the desired peaking factor is achieved. A simple methodology is used to link the field line footprints to the heat load distribution on the target by associating each field line with a constant power value. Characterizing the exact location of the divertor plates is still in progress in order to minimize the heat flux peaking factor. For the engineering effort, a target of 10 MW/m^2 has been identified as design basis.

The operation demands on the divertor are quite high. A high temperature refractory alloy, such as a W alloy, is required to allow for high temperature operation and accommodation of the high heat fluxes and erosion concerns. It is known that the low temperature ductility and the ductile to brittle transition temperature (DBTT) of a tungsten alloy can be dramatically improved by alloying with rhenium. It is assumed that further improvement of the W alloy would allow for a DBTT of 600°C and a recrystallization temperature of $1,300^\circ\text{C}$ under irradiation. However, the waste disposal impact of such an alloy would need to be assessed. The material assumed for the main structure of the divertor targets is advanced ferritic steel, such as the nano-size particle strengthened grade 12YWT. Such type of steel offers reasonable strength properties for an operational temperature up to about 750°C . An important advantage of the stellarator configuration is the absence of major disruption events. Thus, the requirements on the target armor are less demanding than in the case of near-term tokamaks and the thickness of a sacrificial W armor layer depend on the sputtering rate only and expected to be small.

A range of different He-cooled divertor configurations have been considered in the past, including a tungsten plate design. More recently, a finger configuration utilizing tungsten caps has been developed with the aim of minimizing the use of tungsten as structural material and of accommodating higher heat fluxes through the use of smaller units. We have built on this tungsten cap design and explored the possibility of a new mid-size configuration. The proposed configuration consists of a "T-tube" illustrated in Fig. 15.

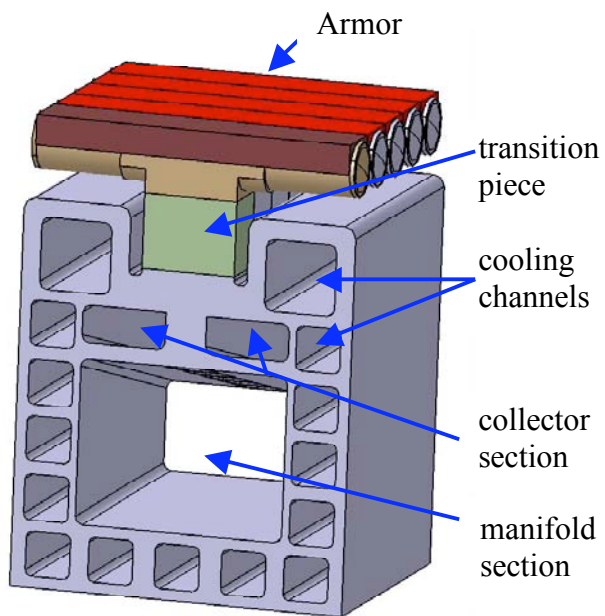
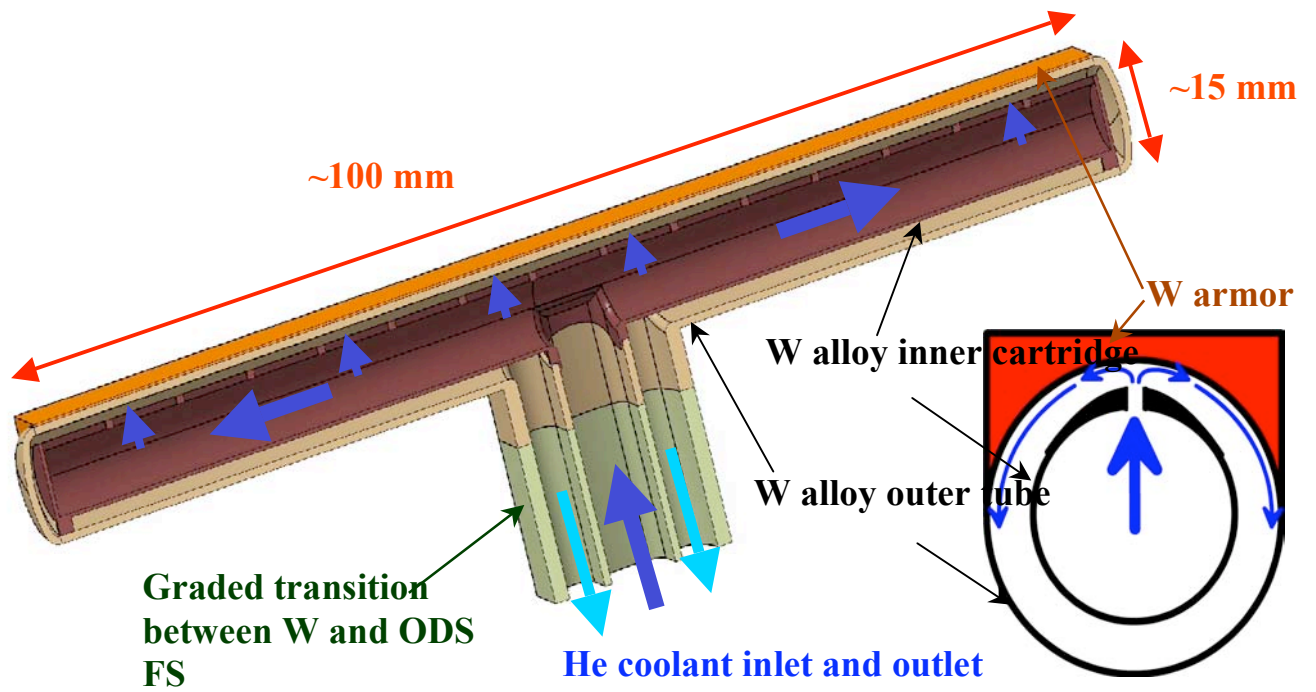


Fig. 15. Schematic of divertor target design with T-tubes (tungsten alloy) integrated with coolant manifold made of advanced ferritic steel.

The T-tube is ~15 mm in diameter and ~100 mm long and is made up of a W-alloy inner cartridge and outer tube on top of which the W armor layer would be attached. The separately fabricated inner cartridge is inserted inside the outer tube and caps are welded at each end. Both W alloy pieces are connected to a base ODS FS unit through a graded transition (*e.g.* using diffusion bonded layers of graded W alloy/ODS FS composition) to minimize thermal stresses. The design provides some flexibility in accommodating the divertor area since a variable number of such T-tubes can be connected to a common manifold to form the desired divertor target, as illustrated in Fig. 15.

The helium coolant is routed through the inner cartridge first and then pushes through thin slots to cool the heat-loaded outer tube surface. A 2D-shaped impinging slot jet is created, leading to high heat transfer at reasonable pressure drop. After impingement, the coolant flows as a highly turbulent wall jet along the large inside surface of the tube and then returns in the lower section of the annular gap between tube and cartridge. As a result of the circular tube cross section and the flat heat flux incidence area, there is a focusing effect on the tube whereby the highest heat flux occurs at the center of the tube and decreases with the angle around the circumference. The cooling characteristics of the jet accommodates this very well as the heat transfer coefficients follow a similar pattern, showing a maximum at the jet impingement location and then decreasing with the angle along the circumference.

Typical parameters for the divertor are summarized in Table 4. The inlet and outlet He temperatures are ~600°C and ~700°C, which fit within the overall heat exchanger and Brayton cycle scheme. A stress analysis was also performed using the ANSYS for an internal helium pressure of 10 MPa and a heat load of 10 MW/m². A 0.3 mm armor layer was assumed bonded to the W alloy surface. The highest stress levels occur in the T-junction area as the T-connector restrains the free bending of the tube. The total stress intensity (primary and secondary stresses) is <370 MPa for the entire geometry (see Fig. 16), which is less than the 3Sm limit of an anticipated W alloy at the corresponding temperatures.

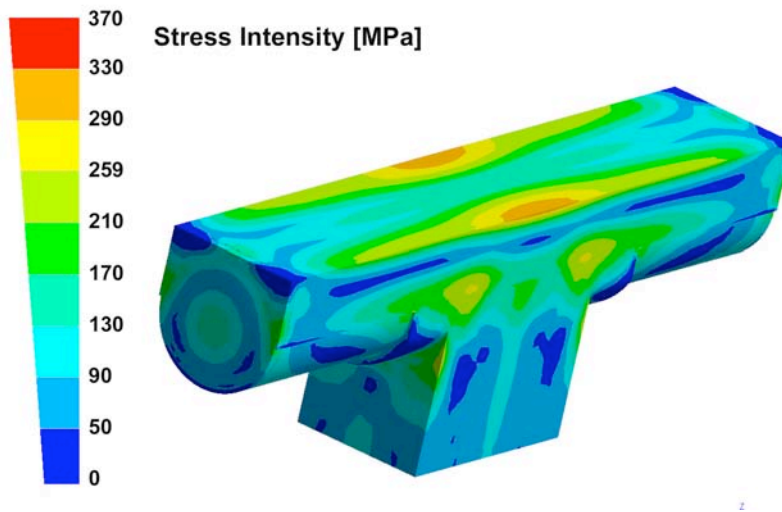


Fig. 14. Stress intensity for the basic divertor T-tube layout and a surface heat flux of 10 MW/m^2 .

Table 4

Summary of Typical ARIES-CS Divertor Parameters for example 3-Field Period CS Configuration

Divertor T-Tube Unit Cell Dimensions	9 cm (tor.) x 1.6 cm (pol.)
He Inlet Temperature	600°C
He Outlet Temperature	700°C
Blanket Inlet Pressure	10 MPa
Typical FW Channel Dimensions	0.5 mm
He Jet Velocity	200 m/s
Average Jet Flow Heat Transfer Coefficient	$\sim 17,000 \text{ W/m}^2\text{-K}$
He Pressure Drop	1 MPa
Total Thermal Power in Divertor	373 MW
Total Mass Flow Rate	730 kg/s
Pumping Power	15.3 MW
Maximum W Alloy Temperature	<1300°C
Maximum Primary + Secondary stresses	<370 MPa

3.5. Alpha-Particle Loss

Because of the inherent non-axisymmetry of the magnetic geometry in a stellarator, a significant magnetic field ripple is present along the flux surfaces inside the plasma and a substantial fraction of α particles may be lost. An important aspect of physics configuration has been the minimization of fast α losses (Sec. 2). We have also used 2 codes to find the location and intensity of α -particle fluxes on the PFCs: ORBIT3D is used to follow the guiding-center or drift orbits of the alphas inside the plasma; outside the LCMS, and the GYRO code which takes into account the gyro-orbit of the particles fully as the gyro-radius of MeV α particles is of the same order as the SOL width.

Loss of fast α particles not only represents a loss of heating power in the core, but more importantly, the PFC must accommodate the heat and particles flux of these high-energy α particles. The high heat flux accommodation could be provided by designing special modules with the divertor geometry discussed in the previous section and which could accommodate up to 10 MW/m². Sputtering is less of a concern and armor lifetime would be governed by some mechanism, such as exfoliation, resulting from accumulation of He atoms in the armor. For an example fusion power of 2,350 MW, a 10% alpha loss and assuming a first wall surface area of 715 m² and an alpha PFC coverage of 5%, the resulting flux on the PFC is $\sim 2.3 \times 10^{18}$ ions/m²-s. For a W armor, the implantation depth for He at ~ 1 MeV is ~ 1.5 μ m. The implanted He would diffuse fairly rapidly through interstitials (with an activation energy of ~ 0.24 eV). However, the presence and/or formation of vacancies, defects or other trapping sites would trap the He, which can then lead to gas-atom precipitation, bubble formation and ultimately to exfoliation and loss of the material. As an example, the He vacancy dissociation energy in W is ~ 4.39 eV. For the above example parameter, the calculated He to W ratio would range from $\sim 10^{-10}$ to ~ 100 for activation energies from 0.24 eV to 4.39 eV, respectively based on a simple estimate of the steady state inventory based on an effective diffusion at 1,400°C. Typically, a He to W ratio of about 0.15 is expected to lead to exfoliation. Clearly, the latter figure indicates that exfoliation would be a major concern. Further experiments and modeling is needed to assess the impact of high-energy α particles on the PFC lifetime.

3.6. Coil Design

The candidate superconductor materials for operation at high field (up to 16 T) are variants of Nb₃Sn. These are glassy material and their current carrying capability is drastically reduced with induced strain. Because of the irregular shape of the coil, the strain induced in the conductor during winding process is too large. Instead, superconductor material should be wound as cable (including the insulator) on the coil and heat treated. This method requires development of inorganic insulators which can withstand the heat

treatment process. Recently, two groups (one in the US, the other one in Europe) have developed glass-tape that can withstand the process in small scale. Extrapolation of this insulator to large coils would allow stellarator magnets with B_{\max} up to 16 T. The strain induced during the winding process is not an issue for ductile NbTi superconductors. However, the maximum field, B_{\max} , is limited to $\sim 7-8$ T for 4 K operation (up to 9 T can be achieved by operation at 2 K although there are issues with temperature margin). Another alternative is development of high-temperature superconductors (HTS), specially YBCO which in principle can be directly deposited on the structural plates as proposed for ARIES-AT.

In a compact stellarator, the absence of disruptions reduces the structural demand on the coil structure. The support structure must accommodate four kinds of static forces acting on the coils: radial forces in the coil plane, large centering forces pulling each coil towards the center of the torus, “out-of-plane” forces acting between neighboring coils inside a field period; and the weight of the cold coil system. Because of the complex shape of the windings, it appears that the best method to support the structural loads is a strong supporting toroidal tube (Figs. 10 & 15). As is shown in Fig. 10 for a three-field period configuration, the cryogenic modular coils are located outside the external vacuum vessel. These coils are wound into grooves at the inside of a strong supporting toroidal tube (see Fig. 15.) which supports the “out-of-plane” or inter-coil forces. This toroidal tube is separable at field periods as there is no net forces (and no force transfer) between each field period. The radial (“in-plane”) forces on the modular coil are supported by strong back. The centering forces can be supported by a bucking cylinder, operated at cryogenic temperature. The weight of the cold supporting tube has to be transferred to foundation by ~ 3 long legs for each field-period. The legs have to be long enough to keep the heat ingress into the cold system within a tolerable limit.

Incoloy 908, with a yield strength of 1,227 MPa at 4 K, is considered as structural material. Initial magnetic and stress analyses were performed using the ANSYS code for scoping the structural thicknesses required to maintain stresses at an acceptable level. The magnetic force calculations confirmed that no net forces are transferred from one field period to the next. On four of the six field-period coils, the net radial force is outward (including the largest force of ~ 222 MN) whereas it is inward for the two other coils. Initial stress analysis using a shell element model indicate a maximum stress of ~ 280 MPa (and a maximum displacement of ~ 0.6 mm) for the initial test-case configuration with an intercoil structure thickness of 0.6 m, a reinforced structure locally behind individual coils of 1.2 m, and a bucking cylinder thickness of ~ 2 m, as shown in Fig. 16. Simple scaling indicates that if a maximum allowable stress of ~ 800 MPa ($\sim 2/3$ the yield strength of incoloy 908) is allowed, the thicknesses could be reduced by a factor of ~ 2.8 . The coil design needs to be finalized based on more detailed analysis of

the specific case including an assessment of the uncertainty associated with the shell element modeling and of the impact of any deflection.

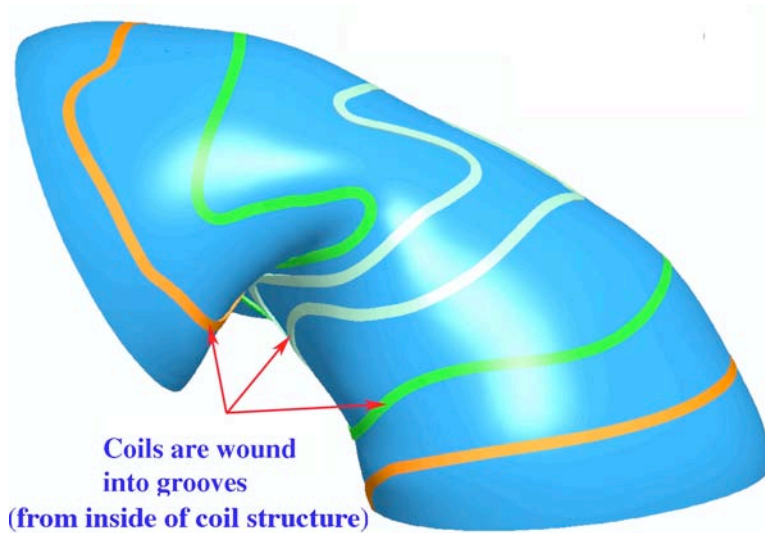


Fig.15. Coil structure for one field period showing the location of the winding pack which is wound from inside the coil. Extra structural thickness would be required behind each coil to react the local force (not shown in the figure)

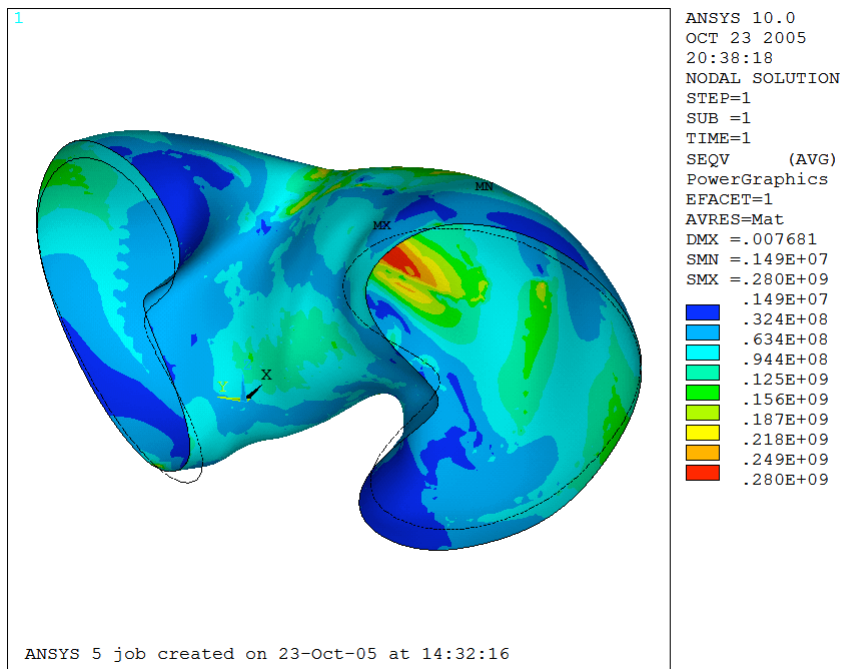


Fig. 16. Initial analysis of Stress results for initial coil test-case analysis

4. SUMMARY

Stellarators have many desirable features as fusion power plants: steady-state operation without externally-driven plasma current (low recirculating power) and stability against external kinks and large vertical displacement events without any feedback coils or conducting walls. A detailed and integrated study of compact stellarator configurations, ARIES-CS, was initiated recently to advance our understanding of attractive compact stellarator power plants and to define key R&D areas. The first phase of the study was devoted to initial exploration of physics and engineering options, requirements, and constraints. In the second phase, we explored the configuration space for stellarators, aiming at configurations that satisfy physics and engineering constraints. The results were reported in this paper.

In the physics area, we have explored several QA configurations. The physics basis of QA as a candidate for compact stellarator reactors has been assessed. New configurations have been developed, others refined and improved, all aimed at low plasma aspect ratios and, hence, compact size at a given fusion power. Configurations with excellent QA have been found with plasma aspect ratios ≤ 4.5 . (Configurations with both 2 and 3 field periods are possible.) Progress has been made to reduce the loss of α particles. It appears that introducing a bias in the principle mirror term in the magnetic spectrum plays an important, but not yet fully understood, role in helping reduce α -particle losses. Numerical calculations using codes based on linear, ideal MHD theories show that stability to the kink, ballooning, and Mercier modes may be attained in most cases but at the expense of reduced QA (and increased α -particle losses) and increased complexity of the plasma shape. Recent experimental results indicate, however, that linear, ideal MHD stability theories may be too pessimistic and not applicable to stellarators.

Previous studies had assumed that the radial build of the fusion core is uniform around the plasma. This is not an optimum approach as the external coils are close to the plasma only in certain locations ($\sim 8\%$ of first-wall surface area) for the NCSX-like configurations. A novel approach was developed in ARIES-CS for these configurations in which the blanket at the critical areas of minimum stand-off is replaced by a highly efficient WC-based shield – *i.e.*, each system has three radial builds: a shield-only region for locations where coils have to be close to the plasma, a nominal blanket and shield for most other locations, and a transition zone in between. In principle, by utilizing the shield-only region in strategic areas, we have been able to reduce the minimum stand-off, Δ_{\min} , by $\sim 30\%$ compared to a uniform radial build that was assumed in previous studies. The reduced Δ_{\min} together with the lower aspect ratio plasma lead to power plants that have similar size as advanced tokamak designs. Table II summarizes the major parameters of a 1,000-MWe power plant based on the NCSX-class configuration N3ARE.

The device configuration, assembly, and maintenance procedures appear to impose severe constraints on the plasma configurations. Modular coils are designed to examine the geometric complexity and to understand the constraints imposed by the maximum allowable field, desirable coil-plasma separation, coil-coil spacing, and other coil parameters. In particular, because of the irregular geometry and small bend radius, development of inorganic insulators is necessary in order to access maximum field of $>9T$. A cost-optimization system code has also been developed and will be utilized to assess the trade-off among physics and engineering constraints during the integrated design phase of the ARIES-CS study.

Major R&D issues specific to compact stellarators that are identified to date include:

- 1) Development and experimental demonstration of compact stellarator configuration with reduced α -particle loss;
- 2) Understanding of β limits in stellarators;
- 3) Demonstration of profile control in compact stellarators to ensure the achievement and control of the desired iota profile, including bootstrap current effects;
- 4) Development and experimental demonstration of “pumped” divertor geometries in compact stellarators;
- 5) Development and experimental demonstration of plasma start-up scenarios and path to ignition with resonance-avoidance techniques;
- 6) Development of high-field superconducting magnets with irregular shape (e.g., in-organic insulators and/or high-temperature superconductors);
- 7) Engineering accommodation of fast α -particle loss.
- 8) Development and demonstration of methods to fabricate, assemble, and maintain large superconducting stellarators free of resonance-inducing field errors.

Documentation

The following papers on ARIES-CS research have been published and/or accepted for the major national and international conferences on fusion energy. In addition, one paper is accepted for the IAEA Fusion Energy conference (2006) and 12 papers are submitted to 17th ANS Topical Meeting on Technology of Fusion Energy (TOFE-17).

1. **"Exploration of Compact Stellarators as Power Plants: Initial Results from ARIES-CS Study,"** F. Najmabadi and the ARIES Team, *Proc. 16th ANS Topical Meeting on the Technology of Fusion Energy (TOFE 16)* (Madison, Wisconsin, September 2004), *Fusion Science & Technology*, **47** (2005).
2. **"Reactors with Stellarator Stability and Tokamak Transport,"** P. Garabedian, L. P. Ku, and the ARIES Team, *Proc. 16th ANS Topical Meeting on the Technology of Fusion Energy (TOFE 16)* (Madison, Wisconsin, September 2004), *Fusion Science & Technology*, **47** (2005).
3. **"Optimization of Stellarator Reactor Parameters,"** J. F. Lyon, L. P. Ku, P. Garabedian, L. El-Guebaly, L. Bromberg, and the ARIES Team, *Proc. 16th ANS Topical Meeting on the Technology of Fusion Energy (TOFE 16)* (Madison, Wisconsin, September 2004), *Fusion Science & Technology*, **47** (2005).
4. **"Attractive Design Approaches for a Compact Stellarator Power,"** A. R. Raffray, L. El-Guebaly, S. Malang, X. Wang, and the ARIES Team, *Proc. 16th ANS Topical Meeting on the Technology of Fusion Energy (TOFE 16)* (Madison, Wisconsin, September 2004), *Fusion Science & Technology*, **47** (2005).
5. **"Ceramic Breeder Blanket for ARIES-CS,"** A. R. Raffray, S. Malang, L. El-Guebaly, X. Wang, and the ARIES Team, *Proc. 16th ANS Topical Meeting on the Technology of Fusion Energy (TOFE 16)* (Madison, Wisconsin, September 2004), *Fusion Science & Technology*, **47** (2005).
6. **"Benefits of Radial Build Minimization and Requirements Imposed on ARIES Compact Stellarator Design,"** L. El-Guebaly, A. R. Raffray, S. Malang, J. F. Lyon, L. P. Ku, and the ARIES Team, *Proc. 16th ANS Topical Meeting on the Technology of Fusion Energy (TOFE 16)* (Madison, Wisconsin, September 2004), *Fusion Science & Technology*, **47** (2005).
7. **"Initial Activation Assessment for ARIES Compact power Plant,"** L. El-Guebaly, P. Wilson, D. Paige, and the ARIES Team, *Proc. 16th ANS Topical Meeting on the Technology of Fusion Energy (TOFE 16)* (Madison, Wisconsin, September 2004), *Fusion Science & Technology*, **47** (2005).

8. **“Design Constraints for Liquid-Protected Divertors,”** S. Shin, S. I. Abdel-Khalik, M. Yoda, and the ARIES Team, *Proc. 16th ANS Topical Meeting on the Technology of Fusion Energy (TOFE 16)* (Madison, Wisconsin, September 2004), *Fusion Science & Technology*, **47** (2005).
9. **“Maintenance Approaches for ARIES-CS Power Plant,”** X. R. Wang, S. Malang, A. R. Raffray, and the ARIES Team, *Proc. 16th ANS Topical Meeting on the Technology of Fusion Energy (TOFE 16)* (Madison, Wisconsin, September 2004), *Fusion Science & Technology*, **47** (2005).
10. **“Three Dimensional Modeling of Complex Fusion Devices Using CAD-MCNPX Interface,”** M. Wang, T. Tautges, D. Henderson, L. El-Guebaly, X. R. Wang *Proc. 16th ANS Topical Meeting on the Technology of Fusion Energy (TOFE 16)* (Madison, Wisconsin, September 2004), *Fusion Science & Technology*, **47** (2005).
11. **“Major Integration Issues in Evolving the Configuration Design Space for the ARIES-CS Compact Stellarator Power Plant,”** A. R. Raffray, S. Malang, L. El-Guebaly, T. Ihli, F. Najmabadi, X. Wang and the ARIES Team, , *Fusion Engineering & Design*, **81**, 1159-1168 (2006).
12. **“Optimization of Compact Stellarator Configuration as Fusion Devices,”** F. Najmabadi, A. R. Raffray, Long-Po Ku, and J. F. Lyon, *Physics of Plasmas*, **13**, 056123(2006) 056123-1 to 056123-12.
13. **“Recent Progress in ARIES compact Stellarator Study,”** F. Najmabadi, A. R. Raffray, and the ARIES Team To appear in *Fusion Engineering & Design*, (2006).
14. **“Accommodation of Prompt Alpha-Particle Loss in Compact Stellarators,”** A. R. Raffray, T. K. Mau, F. Najmabadi and the ARIES Team to appear in *Journal of Nuclear Material* (2006).